JOURNAL OF COMPUTATIONAL PHYSICS 69, 230–251 (1987)

Computation of Anomalous Modes in the Taylor Experiment*

J. H. BOLSTAD† AND H. B. KELLER

Applied Mathematics 217-50, California Institute of Technology, Pasadena, California 91125

Received January 10, 1986

Multigrid continuation methods are used to solve the steady, axisymmetric incompressible Navier–Stokes equations for Taylor–Couette flows between cylinders of finite or infinite length. Using Schaeffer's homotopy, we compute (for finite cylinders) anomalous modes (those seeming to have an odd number of vortices, or seeming to have the "wrong" direction of rotation at an endplate). The results show that these modes possess extra vortices not observed in the experiments of Benjamin and Mullin (*Proc. Roy. Soc. London Ser. A* **377** (1981), 221; *J. Fluid Mech.* **121** (1982), 219). Our computations verify conjectures of Schaeffer, and of Benjamin and Mullin on the unfolding of the bifurcation diagram as periodic (infinite cylinder) flows are continuously transformed to flows with rigid ends. We obtain five distinct solutions with the same Reynolds number, aspect ratio, and radius ratio, and give a systematic procedure for obtaining them. The numerical results show qualitative agreement with the experiments of Benjamin and Mullin. They also show quantitative agreement with the more recent experiments of Cliffe and Mullin (*J. Fluid Mech.* **153** (1985), 243).

1. INTRODUCTION

The experiments of Benjamin and Mullin [1, 2, 3] revived interest in the Taylor vortex problem, first studied by G. I. Taylor in 1923 [27]. They also stimulated interest in computations of problems with multiple solutions.

In these experiments the inner cylinder rotates and the outer cylinder and top and bottom endplates are fixed. The fluid is thrown outward by centrifugal force. The no-slip condition retards this outward motion near the top and bottom, so one normally expects the outward flow to be greatest midway between the top and bottom (hereafter called the midplane). Hence, if the flow contains Taylor vortices, one expects the flow to be *inward* near the top and bottom, and *outward* at the mid-

* This work was supported by the U. S. Department of Energy under Contracts EY-76-S-03-070 and W-7405-ENG-48, by the U.S. Army Research Office under Contract DAAG-29-78-C-0011, and by the U.S. Air Force under Grant AFOSR-82-0321.

† Present address: Lawrence Livermore National Laboratory, Box 808 L-16, Livermore, California 94550.

0021-9991/87 $3.00

plane. This is exactly what is observed in what Benjamin and Mullin call the "normal" modes (e.g., Fig. 4(a)). These modes or primary flows are the ones which can be experimentally generated by starting the apparatus at low Reynolds number (rotation rate of the inner cylinder), and slowly increasing it. Symmetry arguments also suggest that Taylor vortex flows should possess an *even* number of cells.

In 1981 Benjamin and Mullin [2] reported experiments which showed what they called *anomalous modes*: stable Taylor vortex flows "that exist only at sufficiently high Reynolds number R and are always distinct from the primary flow..." These anomalous modes *seem* to have an odd number of Taylor vortices and/or *seem* to have cells adjacent to the end plates spiraling in the "wrong" direction. We prefer this latter description of anomalous although the definition of Benjamin and Mullin may be broader and could include flows not yet observed or computed. They also suggested a bifurcation diagram for the "anomalous two modes," i.e., those which appeared to have two cells.

Benjamin and Mullin's construction of the bifurcation diagram was based on the work of Schaeffer [24]. His analysis proceeds directly from the steady, incompressible Navier–Stokes equations. Schaeffer started from the well-known bifurcation diagram for infinite cylinder (periodic) flow. He introduced a homotopy (given in Sect. 2) between the infinite cylinder and finite cylinder problems. The homotopy parameter value $\tau = 0$ gives the former and $\tau = 1$ gives the latter. Schaeffer studied the change in the bifurcation diagram as τ is increased from zero. At $\tau = 0$ this is just perturbed bifurcation theory. He then made the assumption that the behavior obtained for "small" τ was qualitatively the same as the behavior for $\tau = 1$, i.e., finite cylinder flow. His work applied to configurations with an even number $n > 2$ of vortices and explained the existence of cusps and hence of hysteresis effects. For technical reasons his results did not apply to two-vortex flows. However, Benjamin and Mullin [2] employed Schaeffer's homotopy and unfolding arguments to explain the anomalous modes they observed for two-vortex flows.

The results of this paper are fourfold. First, our computations show that the anomalous modes all contain additional "hidden" vortices apparently not observed or not reported by Benjamin and Mullin. These vortices are much smaller and weaker than the ones they observed. When these "hidden" vortices appear in the flow pictures (contours of the stream function) all suggestions of "wrong" direction of rotation or of odd numbers of vortices disappear. (A similar result was obtained by Cliffe [9] for so-called one-vortex flows.)

Second, we numerically implement the homotopy of Schaeffer. We find, as both Schaeffer and Benjamin and Mullin assumed, that the bifurcation diagram for small τ is qualitatively the same as that for $\tau = 1$. Indeed it was not even clear before that the homotopy existed for the entire interval, $0 \leqslant \tau \leqslant 1$. We use this homotopy to start from a two-cell mode for infinite cylinders and obtain an anomalous two-cell mode for finite cylinders. The operation of this homotopy is illustrated here for the first time (Fig. 3). Then we use this finite cylinder solution to trace out (using continuation methods) the entire bifurcation diagram which Benjamin and Mullin

proposed for the two-cell modes. We thus numerically confirm their bifurcation diagram.

Third, our implementation of the homotopy provides a systematic procedure for obtaining anomalous modes. Benjamin and Mullin's bifurcation diagram has the anomalous modes *disconnected* from the "normal" modes. Thus, if this is the correct picture, ordinary continuation (in the Reynolds number or the aspect ratio) from the normal modes will not succeed in locating the anomalous modes. We compute anomalous n cell modes for $n=2$ through 6. For $n=2$ we show five distinct solutions of the Taylor problem with the same Reynolds number, aspect ratio, and radius ratio.

Fourth, we compute the locus of fold points with respect to Reynolds number as the aspect ratio is varied (i.e., a fold in the "sheet" of solutions above the plane of aspect ratio and Reynolds number). We discover new geometric features in the 5- and 6-mode folds. We also see that the "hidden" vortices in the 2-mode at low aspect ratios each split into two subvortices. Our results agree qualitatively with the folds located experimentally by Benjamin and Mullin, but there is a 30% quantitative disagreement.

After obtaining these results (a preliminary version of which was reported in [4]) we received a report by Cliffe and Mullin [10] in which they independently calculated some of the anomalous modes by using Schaeffer's homotopy. They also conducted new experiments in which they observed the "hidden" vortices. In the process they discovered that the old experiments were incorrect by 30%. Our results show good agreement with their new experiments and with their computaions.

Other recent computations of Taylor vortex flows are as follows. Time-dependent computations were performed by Neitzel [23] and by Fasel and Booz [13] for axisymmetric flows in finite cylinders, and by Marcus [19] for flows in infinite cylinders. Steady, axisymmetric flows have been computed by Meyer–Spasche and Keller [21, 22] for infinite cylinders, and for finite cylinders by Cliffe and co-workers [9, 10, 11, 17] and by Strikwerda [25].

Finally, some comments on two points of terminology are in order. Families of solutions of nonlinear problems in which one parameter varies are said to have "fold points," "limit points," "turning points," or "one-sided bifurcations." These are all meant to describe the same behavior (and the latter two phrases are most unfortunate). If the problems depend upon two or more parameters we can fix all but one of the parameters, say λ, and then have a fold or limit point with respect to λ. If now a second parameter is allowed to vary, the fold point sweeps out a curve of folds or simply a "fold" (in the two-parameter plane).

We know that the so-called one-cell modes actually contain two cells [9]. Furthermore, we now know that the "anomalous two modes" (cf. Fig. 4) and "anomalous three modes" (Fig. 5) which Benjamin and Mullin observed actually contain four cells. Nevertheless it is frequently convenient to retain the original terminology in order to distinguish these quite distinct flows. At other times we shall refer to them as anomalous flows with four vortices (or cells).

2. Formulation

The experimental setup employs a pair of concentric circular cylinders of radii R_1 and R_2, $R_1 < R_2$, and length L, with rigid end walls fastened to the outer cylinder. The gap between the cylinders is filled with viscous incompressible fluid of kinematic viscosity ν, and the inner cylinder rotates about the common axis with angular velocity Ω. The outer cylinder and ends are at rest. The flow is assumed to be steady and axisymmetric.

We use cylindrical polar coordinates (r, θ, z) with corresponding velocities (u, v, w). The origin of coordinates is at the intersection of the axis of rotation with the plane passing through the bottom of the annulus.

The variables are made dimensionless by using the gap width $d = R_2 - R_1$ and the velocity ΩR_1 of the inner cylinder as reference length and velocity, respectively. The problem is characterized by three dimensionless parameters: the Reynolds number $R = \Omega R_1 d/\nu$ based on gap width, the aspect ratio $\Gamma = L/d$, and the radius ratio $\eta = R_1/R_2$. Using the Stokes stream function, the Navier–Stokes equations can be reduced to (Goldstein [16])

$$2v\frac{\partial v}{\partial z} + \frac{1}{r}\frac{\partial(\psi, D^2\psi)}{\partial(r, z)} + \frac{2}{r^2}\frac{\partial \psi}{\partial z}D^2\psi - \frac{1}{R}D^4\psi = 0, \tag{2.1}$$

$$\frac{1}{r^2}\frac{\partial(\psi, rv)}{\partial(r, z)} - \frac{1}{R}\left(\nabla^2 v - \frac{v}{r^2}\right) = 0. \tag{2.2}$$

Here the swirl operator D^2 is introduced as

$$D^2 \equiv r\frac{\partial}{\partial r}\frac{1}{r}\frac{\partial}{\partial r} + \frac{\partial^2}{\partial z^2},$$

the Laplacian is

$$\nabla^2 \equiv \frac{1}{r}\frac{\partial}{\partial r}r\frac{\partial}{\partial r} + \frac{\partial^2}{\partial z^2},$$

and the Jacobian is

$$\frac{\partial(f, g)}{\partial(r, z)} \equiv f_r g_z - f_z g_r.$$

The equations are to be solved in the annulus

$$\rho \leqslant r \leqslant \rho + 1, \qquad 0 \leqslant z \leqslant \Gamma,$$

where $\rho = \eta/(1-\eta)$. The radial and axial velocities are given by

$$u = -\frac{1}{r}\frac{\partial \psi}{\partial z} \qquad \text{and} \qquad w = \frac{1}{r}\frac{\partial \psi}{\partial r}, \tag{2.3}$$

respectively.

The boundary conditions on the cylindrical surfaces are

$$\psi = \partial\psi/\partial n = 0 \qquad \text{at } r = \rho, \rho + 1; \tag{2.4}$$

$$v = 1 \qquad \text{at } r = \rho; \tag{2.5}$$

$$v = 0 \qquad \text{at } r = \rho + 1. \tag{2.6}$$

Here $\partial/\partial n$ denotes the outward normal derivative.

At the bottom $z = 0$ and top $z = \Gamma$ we prescribe, following Schaeffer [24], a one-parameter family of boundary conditions depending on a *homotopy parameter* τ,

$$\psi = 0, \tag{2.7}$$

$$(1 - \tau)\, \partial^2\psi/\partial n^2 + \tau\partial\psi/\partial n = 0, \tag{2.8}$$

$$(1 - \tau)\, \partial v/\partial n + \tau v = 0. \tag{2.9}$$

The value $\tau = 1$ describes finite cylinders, and $\tau = 0$ gives what Schaeffer calls *quasi-periodic* (in z) boundary conditions. A solution (ψ, v) with quasi-periodic boundary conditions is related to one with *periodic* (in z) boundary conditions in one of two ways. Either the former is the same as the latter; or else, a solution of the former defined for $0 \leqslant z \leqslant \Gamma$ can be extended to a solution with periodic boundary conditions over $-\Gamma \leqslant z \leqslant \Gamma$ by defining ψ (resp. v) as an odd (even) function of z. Thus a quasi-periodic solution can contain an odd number of vortices but a periodic solution cannot. These boundary conditions provide a continuous deformation (or homotopy) of the periodic flows into flows with experimentally realistic end conditions.

After the stream function and azimuthal velocity are determined, we calculate the pressure by solving a Poisson equation (in cylindrical coordinates)

$$-\Delta p = u_r^2 + \frac{u^2}{r^2} - \frac{1}{r}\frac{\partial}{\partial r} v^2 + 2u_z w_r + w_z^2$$

subject to Neumann boundary conditions, with u and w given by (2.3). This equation is derived by taking the divergence of the u and w momentum equations. The boundary conditions come from evaluating these momentum equations on the boundaries.

The above equations are used for flows which appear to have no symmetry in z. For flows such as "normal modes" and anomalous modes with an even number of cells, we compute on only half the domain $0 \leqslant z \leqslant \Gamma/2$, changing only the boundary conditions at the midplane $z = \Gamma/2$. We use (2.8) and (2.9) at $z = \Gamma/2$, but with τ replaced by 0, regardless of the actual value of τ. We also replace the pressure boundary condition here by $\partial p/\partial n = 0$.

The (θ component of the) vorticity is determined by taking the swirl of the stream function:

$$\zeta = -\frac{1}{r} D^2\psi.$$

3. Numerical Methods

Equations (2.1), (2.2) are discretized on a sequence of uniform grids using second order centered finite differences.

Let N_r and N_z be the number of grid intervals in the r and z directions, respectively. Define the step sizes $\Delta r = 1/N_r$ and $\Delta z = \Gamma/N_z$ ($\Delta z = \Gamma/2N_z$ for a symmetric solution on half the region). The radial step Δr need not equal the axial step Δz. Let $r_i = \rho + i\Delta r$ and $z_j = j\Delta z$. Let $\psi_{i,j}$ and $v_{i,j}$ approximate ψ and v at (r_i, z_j). The discretizations of (2.1) and (2.2) are imposed for $i = 1, 2, \ldots, N_r - 1$. To define the j range, let the bottom index B be 0 if $\tau \neq 1$ and 1 if $\tau = 1$. Let the top index T be N_z if $\tau \neq 1$ or if the solution is symmetric in z, and $N_z - 1$ otherwise. Then the discretization of (2.1) is imposed for $j = 1, 2, \ldots, N_z - 1$, while that of (2.2) is imposed for $j = B$ to T.

The differencing of the differential equations is straightforward. We discretize (2.2) as

$$\frac{1}{4r_i^2 \Delta r \Delta z}\left[r_i(\psi_{i+1,j} - \psi_{i-1,j})(v_{i,j+1} - v_{i,j-1}) - (\psi_{i,j+1} - \psi_{i,j-1})(r_{i+1} v_{i+1,j} - r_{i-1} v_{i-1,j})\right] - \frac{1}{R}\left[\frac{r_{i+1/2} v_{i+1,j} - 2r_i v_{i,j} + r_{i-1/2} v_{i-1,j}}{r_i (\Delta r)^2} + \frac{v_{i,j+1} - 2v_{i,j} + v_{i,j-1}}{(\Delta z)^2} - \frac{v_{i,j}}{r_i^2}\right] = 0.$$

The differencing of (2.1) is equally straightforward but very complicated. The stencil occupies 13 points.

For the Neumann boundary conditions (2.4), (2.8), (2.9) we introduce image points outside the region (at $i = -1$ and $N_r + 1$ and at $j = -1$ and $N_z + 1$) and also use centered second order approximations. These equations are used to eliminate the image points from the discretizations of (2.1) and (2.2).

The resulting discretized equations can then be written as a system of $(N_r - 1)(N_z + T - B)$ nonlinear algebraic equations depending on four parameters

$$G(\mathbf{u}; R, \Gamma, \eta, \tau) = 0. \tag{3.1}$$

Here $\mathbf{u}$ is a vector whose components are the inerlaced values $\psi_{i,j}$ and $v_{i,j}$, ordered first in increasing i and then in increasing j. This system is solved using Euler–Newton pseudo-arclength continuation [18]. Generally we hold three parameters constant and vary the fourth, except during fold-following, to be discussed below, when two parameters are held constant and two are varied.

A disadvantage of this procedure is that considerable storage is required for the Jacobian G_u of the system (3.1). (Here G_u is a large block pentadiagonal matrix.) To circumvent this difficulty we combine continuation with the multigrid method [6]. Our method uses the *full, accommodative* multigrid method with the *full approximation scheme*. (See Brandt [6] for definitions of these terms.) For

smoothing on all but the coarsest grid we use *alternating zebra* (alternating line or block) Gauss–Seidel–Newton relaxation [26]. The usual 9-point operator is used to project residuals onto coarser grids.

The multigrid method employs a nested sequence of grids over the same region. Each grid typically has a grid spacing which is half the grid spacing of its predecessor. Thus in a typical run, the finest grid may have 80 r-intervals by 160 z-intervals, while the coarsest grid may have only 5 r-intervals by 10 z-intervals. Our multigrid continuation method [5] combines the frozen tau technique [6] with pseudo-arclength continuation and correction of the continuation parameter on the coarsest grid. As a result, we need store the Jacobian G_u *only on the coarsest grid*, and this produces considerable storage savings.

A difficulty with the multigrid method for singular perturbation problems in the range of Reynolds numbers that we consider is that the solution may be well resolved on the finest grid, but poorly resolved on coarser grids. The result is divergence of the multigrid iteration. To circumvent this we use a "double discretization" method [6]: on all but the finest grid we add an artificial viscosity to the smoothing operator but not to the coarse grid residual transfer operator. This preserves the second order accuracy of the scheme.

The pressure equation is solved using multigrid but not continuation. Since the Neumann problem is singular, we must ensure that the discrete problem satisfies an appropriate consistency condition (derivable from a discrete Green's Theorem). We smooth using checkerboard Gauss–Seidel. The coarse grid equations are solved directly after discarding one equation to make the system nonsingular. The arbitrary solution constant is chosen by prescribing the (discrete) average pressure to be zero.

To compare our results with the experiments of Benjamin and Mullin, we employed the following "fold-following" procedure. Each anomalous mode has a fold (or limit) point with respect to Reynolds number. As the aspect ratio is varied, we obtain a locus of such points, or a *fold* in a "sheet" of solutions. These folds give the approximate parameter values where the experimental anomalous modes lose stability and hence collapse. To continue along the fold in the (Γ, R)-plane, we fix the parameters η and τ, and use Euler–Newton pseudo-arclength continuation for an augmented system of nonlinear equations. This method is due to Fier and Keller [14, 15]. Another method has been given by Moore and Spence [22].

The augmented system is

$$G(\mathbf{u}; R, \Gamma) = 0, \tag{3.2a}$$

$$G_u^* \Psi = 0, \tag{3.2b}$$

$$G_R^* \Psi = \text{constant}, \tag{3.2c}$$

together with the normalization condition for arclength parametrization

$$\langle \dot{\mathbf{u}}, \dot{\mathbf{u}} \rangle + \dot{R}^2 + \dot{\Gamma}^2 = 1,$$

or for pseudo-arclength parametrization

$$\langle \dot{\mathbf{u}}, \mathbf{u}-\mathbf{u}_0 \rangle + \dot{R}(R-R_0) + \dot{\Gamma}(\Gamma-\Gamma_0) = s - s_0. \tag{3.3}$$

The former normalization is used for the Euler step and the latter is used for the Newton iterations. Here G_u denotes the Jacobian matrix at the point $P = \{\mathbf{u}_0; R_0, \Gamma_0\}$, * denotes the adjoint (or matrix transpose), Ψ^* is the left null vector of the Jacobian at P, s is the pseudo-arclength parameter, "$\cdot$" denotes $\partial/\partial s$ evaluated at P, and $\langle\ ,\ \rangle$ denotes the usual discrete L_2 inner product approximating the continuous one. Note that Ψ does not appear in the normalization conditions. The system of equations for the Newton iterates is obtained by expansion of (3.2), (3.3) with respect to small changes in $\mathbf{u}$, R, Γ, and Ψ. This leads to a system of linear equations for the changes: $\mathbf{u}-\mathbf{u}_0$, $\Psi-\Psi_0$, $R-R_0$, and $\Gamma-\Gamma_0$. The solution of the augmented linear system can be obtained by solving three bordered systems. This, in turn, requires the solution of three systems with matrix G_u and two systems with matrix G_u^*. The Euler step requires the solution of one system with matrix G_u and one with matrix G_u^*. Finite differences are used to approximate second derivatives such as G_{uu} or G_{uR}.

This algorithm is implemented with the aid of the bandsolver DGBCO/SL/DI in LINPACK [12]. LINPACK allows the solution of systems with matrices G_u or G_u^* so we require only one factorization of the Jacobian G_u per Euler or Newton step. The condition estimator in LINPACK is useful to verify that we stay on the fold, since the determinant cannot be used here. Furthermore, the condition estimator supplies the right null vector and is trivially modified to supply the left null vector Ψ of G_u, both of which are required in the Euler step. (This is not surprising, since the condition estimator effectively performs one inverse iteration with each of matrices G_u and G_u^*.) An advantage of this method is that it can be implemented using only slightly more storage than pseudo-arclength continuation in one parameter. But we have not yet tried to combine this algorithm with the multigrid method.

Our formulation of Eq. (3.2c) differs from that in [14, 15] where the constant is set to one. We choose our constant before each Euler step by suitably normalizing the left null vector Ψ from LINPACK (by letting its discrete L_2 norm equal 1), and setting the constant equal to the left side of (3.2c). The constant is fixed until we converge to the next fold point. Using the formulation in [14, 15] leads to a badly scaled Ψ in our problem.

4. Computing Anomalous Modes by Continuation

In this section we will describe the structure of the bifurcation diagram for the anomalous two-modes, and show how it is related to the bifurcation diagram for periodic flows. Then we will explain how we use continuation to compute anomalous n-cell modes for $n \geqslant 2$. We have employed this algorithm for $n = 2, 3, 4, 5$, and 6.

The structure of these bifurcation diagrams was first analyzed by Schaeffer [24] for flows with an even number of cells, and by Benjamin and Mullin [2] for the interaction of an N cell and an $N+1$ cell mode. Figure 1 shows a schematic bifurcation diagram of one and two cell quasi-periodic flows ($\tau = 0$) for an aspect ratio Γ near one. Couette flow (shown as lying on the R axis) bifurcates into one-cell and two-cell flows at pitchfork bifurcation points P_1 and P_2, respectively. The points S_1 and S_2 are secondary (pitchfork) bifurcation points for the two-cell flows.

Following [2], we now explain the symmetry axes A and S in Fig. 1 and 2. Let Couette flow have velocity components $(u, v, w) = (0, v_0, 0)$. Two symmetry classes can be distinguished for quasi-periodic flows: the "class (i)" or "symmetric" flows, for which the velocities u and v are even (symmetric) about the midplane $z = \Gamma/2$ while w and ψ are odd (antisymmetric); and the "class (ii)" or "antisymmetric" solutions, with u, $v - v_0$, w, and ψ, respectively, odd, odd, even, and even about the midplane. The axes then indicate that a point which lies in the (R, S) plane has no antisymmetric component, while a point which lies in the (R, A) plane has no symmetric component. Thus the flows in Fig. 1 which issue from the top or bottom prongs of the secondary pitchfork bifurcation points S_1 and S_2 are neither symmetric nor antisymmetric.

The main idea in [24] and [2] for analyzing the flows is to increase the aspect ratio until the points P_1 and P_2 coalesce, and use the methods of bifurcation theory to explain the behavior of the bifurcation diagram for "small" τ and for P_1 near P_2. The primary bifurcation at P_2 is split, but the others are not because of the sym-

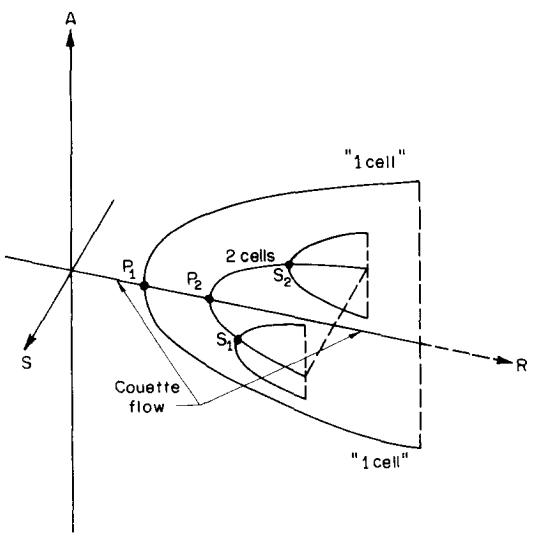

FIG. 1. Schematic bifurcation diagram for one and two cell quasi-periodic flows. Couette flow bifurcates into one-cell and two-cell flows at points P_1 and P_2, respectively. The points S_1 and S_2 are secondary bifurcation points for the two-cell flows. The S and A axes are related to the symmetry (in z) of the flows (see text).

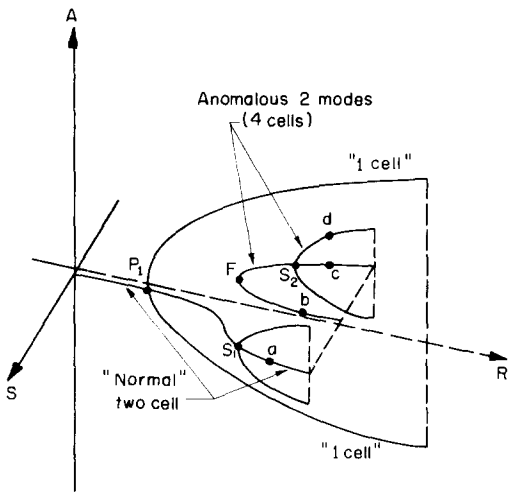

FIG. 2. Schematic bifurcation diagram for "normal" two cell, "one cell," and "anomalous two cell" finite cylinder flows. The "one cell" flow actually contains two unequal cells. The "anomalous two cell" flows in fact consist of four cells. The primary bifurcation point P_2 in Fig. 1 has been split, resulting in a solution branch (the anomalous modes) which is *disconnected* from the branch of the normal two cell modes.

metry. Assuming that the qualitative behavior of the bifurcation diagram is the same for "small" τ as for $\tau = 1$, Benjamin and Mullin [2] obtained the schematic bifurcation diagram for finite cylinder flows in Fig. 2. Here the positive R axis, shown dotted for clarity, is not part of a flow. Couette flow in Fig. 1 has been transformed into "normal" two-cell flow. The one-cell quasi-periodic flows of Fig. 1 have become the so-called "one-cell" finite cylinder flows, and actually contain two unequal cells [9]. The primary bifurcation point P_2 in Fig. 1 has been split, resulting in a solution branch (the anomalous modes) which is *disconnected* from the branch of the normal two cell modes. As we shall see, the "anomalous two-cell" flows in fact consist of four cells. The figure is meant to show that symmetric finite cylinder flows exist, but antisymmetric ones cannot. Moreover, if $(\psi(z), v(z))$ is a solution, then so is $(-\psi(\Gamma - z), v(\Gamma - z))$. Thus, the image in the (R, S) plane of any solution is also a solution. These facts are evident from the differential equations and boundary conditions.

Our strategy for systematically computing anomalous modes is as follows. We start with Couette flow with quasi-periodic boundary conditions ($\tau = 0$) at small Reynolds number (e.g., 20). If we desire an n-cell anomalous mode, we set the aspect ratio to n. Then we continue in Reynolds number, increasing until we reach the first bifurcation point. (This is detectable by a change in the sign of the determinant of the Jacobian G_u. The techniques for detecting, and switching branches at bifurcation points are by now standard [18].) It will be a (supercritical) pitchfork bifurcation from Couette flow into an n-cell quasi-periodic flow. Of the two possible bifurcating branches, we continue from the one with cells whose direction of flow

nearest the $z = 0$ and $z = \Gamma$ ends is outward (towards the outer cylinder) when n is even. Equivalently, the desired branch has a negative radial velocity u at the center $(r, z) = (\rho + \frac{1}{2}, \Gamma/2)$ of the annulus. (If we continue from the other branch, we will obtain normal modes for finite cylinders.) When n is odd, we can follow either branch, since we will obtain finite cylinder anomalous modes in both cases. (The branching direction from the bifurcation point is given by the right null vector of the Jacobian G_u, which can be calculated cheaply from the matrix factorization of G_u [18].) Next we continue in Reynolds number on the appropriate bifurcated branch, increasing until approximately $R = 250$. Then we switch from quasi-periodic to finite cylinder flow by fixing the Reynolds number and continuing in increasing τ (the boundary homotopy parameter) from 0 to 1.

The birth of hidden vortices by continuation in τ is illustrated in Figs. 3a–e for $n = 2$ at five values of τ. The contour plots show the intersection of the annulus with the (r, z) plane through the axis of rotation, with the inner (rotating) cylinder at the left. Stream function contours are shown above and vorticity contours below in part 1 of the figure, and azimuthal velocity contours are shown in part 2 of the figure. The solutions were computed by multigrid continuation on a 65×65 grid (on half the region, using symmetry) at Reynolds number 240, aspect ratio 2, and radius ratio 0.615. This radius ratio is the one used in the experiments of Benjamin and Mullin, and the computations of Cliffe and Mullin, and is used in all computations in this paper. All contour plots in this paper are drawn with their true aspect ratios. The respective values of τ are 0, 0.5, 0.7, 0.8, and 1.0. The azimuthal velocity contours clearly show the change in the boundary conditions at top and bottom. When n is even (odd) we see two (one) extra vortice(s) forming at the end(s) $z = 0$ and $z = \Gamma$. If one looks only at stream function contours, the extra vortice(s) do not seem to appear until $\tau = 0.8$. (The zero stream function contours, across which the (r, z) flow reverses, are those which intersect the boundaries.) However, the vorticity plots reveal incipient vortices as early as $\tau = 0.50$. (The same early behavior is shown by contour plots of radial or axial velocity.) For $n = 3$ this behavior occurs for the same values of τ. Indeed, in all the cases we tried, the extra vortices did not form fully until $\tau = 0.8$ or later. Since these new features occur for relatively large τ values, they could not have been determined by perturbation calculations about $\tau = 0$. Thus Benjamin and Mullin could have had no theoretical evidence to explain the fate of the anomalous modes for $n = 2$.

The algorithm for $n = 2$ can be related to Figs. 1 and 2, with one slight change. As mentioned, these figures were drawn for an aspect ratio near one, rather than two as in our algorithm. To apply the algorithm to Fig. 1, we start with Couette flow and continue in increasing Reynolds number until we reach the *second* bifurcation point P_2. We take the branch in the negative S direction and follow it a "sufficient" distance (say $R = 250$), possibly but not necessarily past the bifurcation point S_2. Then we fix R and continue in τ from 0 to 1. We will arrive on the branch of anomalous modes in the (R, S) plane of Fig. 2. Depending on the aspect ratio and Reynolds number, we may arrive near point b, F, S_2, or c. For $n = 2$ we happened to arrive at point b.

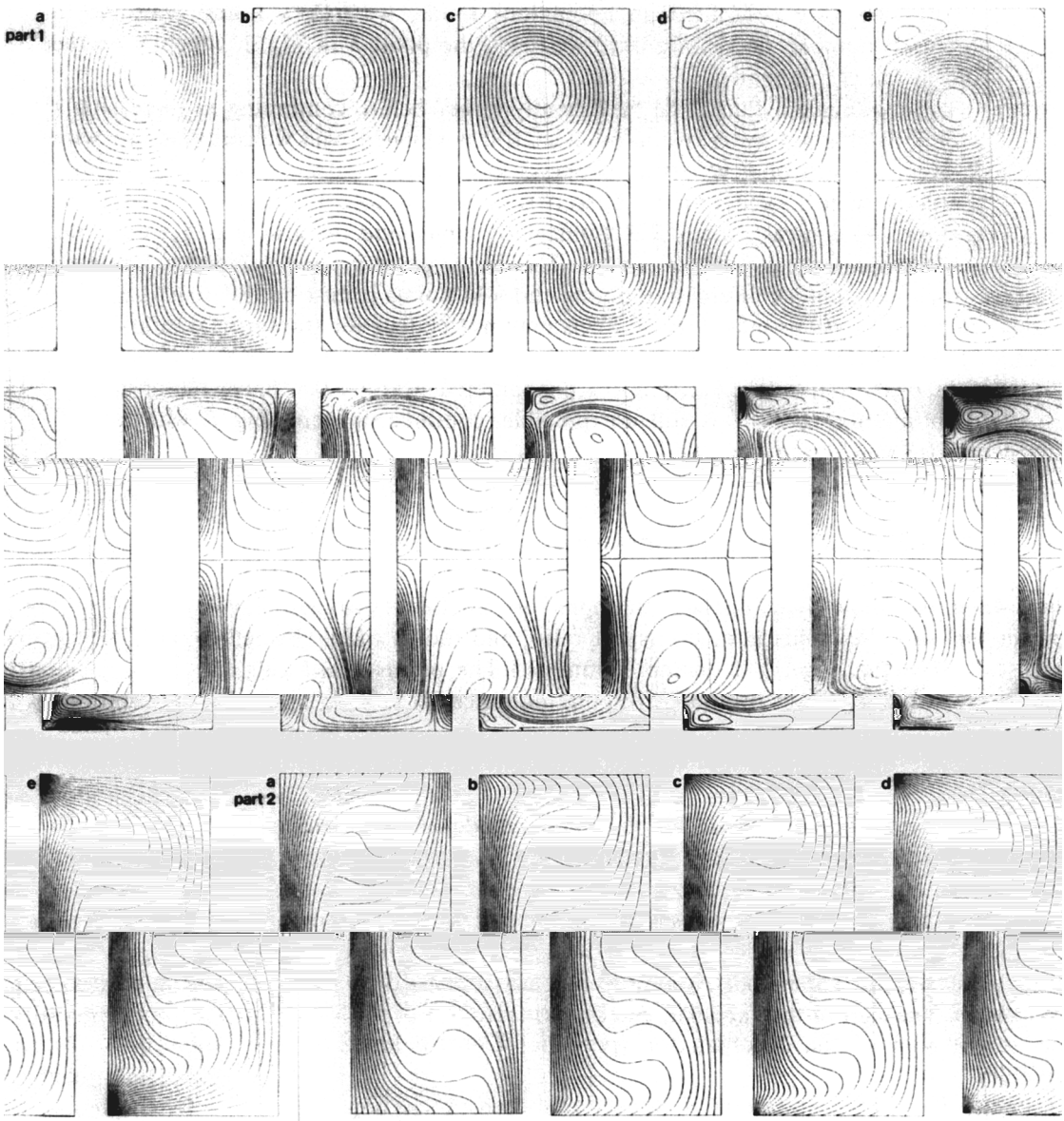

FIG. 3. Transformation from quasi-periodic two-cell flow to anomalous two-cell finite cylinder flow by variation of the boundary homotopy parameter τ. The contour plots show the intersection of the annulus with the (r, z) plane through the axis of rotation, with the inner (rotating) cylinder at the left. The solutions are computed by multigrid continuation on a 65×65 grid (using symmetry in z) at Reynolds number 240, aspect ratio 2, and radius ratio 0.615. Part 1: Above are contours of stream function and below are contours of vorticity. Part 2: Contours of azimuthal velocity. Throughout this paper, all contours are equally spaced in the respective variable, except that the zero contour is always included. (a) $\tau = 0$ (quasi-periodic); (b) $\tau = 0.50$; (c) $\tau = 0.70$; (d) $\tau = 0.80$; (e) $\tau = 1$ (finite cylinder).

After we have computed an anomalous mode, we fix $\tau = 1$ and continue in Reynolds number, decreasing until we reach the point F in Fig. 2, which is on the fold in the (Γ, R) plane.

The requirement that R be "sufficiently large" before continuing in increasing τ with R fixed is not restrictive in practice. If it is violated, and we continue in τ with R fixed, we will observe extra vortice(s) form near $\tau = 0.8$, as before, but a fold (limit) point in τ occurs for $\tau < 1$, so it is impossible to continue to $\tau = 1$ with this grid size. In contrast, when R is "sufficiently large" and the grid is sufficiently fine, the same fold point occurs for $\tau > 1$. This illustrates a general principle: geometric features such as pitchfork bifurcation points and fold points persist on different size grids, but their locations may change. (This may not be true for transcritical bifurcations.) The strategy, then is to start on a very coarse grid: $8 \times 8n$ for an anomalous n-cell mode. If a fold point is encountered near $\tau = 0.8$, halve the grid size. If continuation to $\tau = 1$ is still not possible, continue in increasing R with τ fixed near 0.8 and repeat.

5. Numerical Results and Comparison with Experiments

In Figs. 4a–d we show four distinct solutions of the finite cylinder Taylor problem for the same Reynolds number, aspect ratio, and radius ratio. (By reflection in case d, we actually get five distinct solutions.) The points at which these solutions were evaluated are indicated by the corresponding letters in Fig. 2. The parameters are the same as in the previous section, expect that the homotopy parameter $\tau = 1$, and we did not take advantage of the symmetry so that we could determine stability.

Figure 4a shows the normal two-cell mode for the finite cylinder. This is easily obtained by starting with Reynolds number 20 (where there is a unique solution which can be obtained using a zero initial guess) for finite cylinders and continuing in increasing Reynolds number. (The small lines in the upper and lower right-hand corners of the stream function plots are anomalies of the contour plotting routine.) Figure 4b (the same as 3e) shows the anomalous two-mode that was obtained by the procedure outlined above. The sign of the Jacobian determinant $\det(G_u)$ of this solution is the same as the sign of the Jacobian for (periodic) Couette flow, indicating possible stability.

By continuing to decrease R until the fold point is reached and then proceeding to increase R on the other branch, we first encounter a secondary pitchfork bifurcation point (Fig. 2). If we then continue on the middle branch of the pitchfork, we obtain Fig. 4c. The sign of the Jacobian of this solution is the same as before (by exchange of stability). Finally, Fig. 4d shows an anomalous mode which is unsymmetric in z, and is thus on the top or bottom prong of the pitchfork. There is another solution symmetrically located on the other prong, obtained by reflection in z. Both of these solutions have opposite stability from the previous solutions (by either exchange of stability or our numerical results) and thus are unstable.

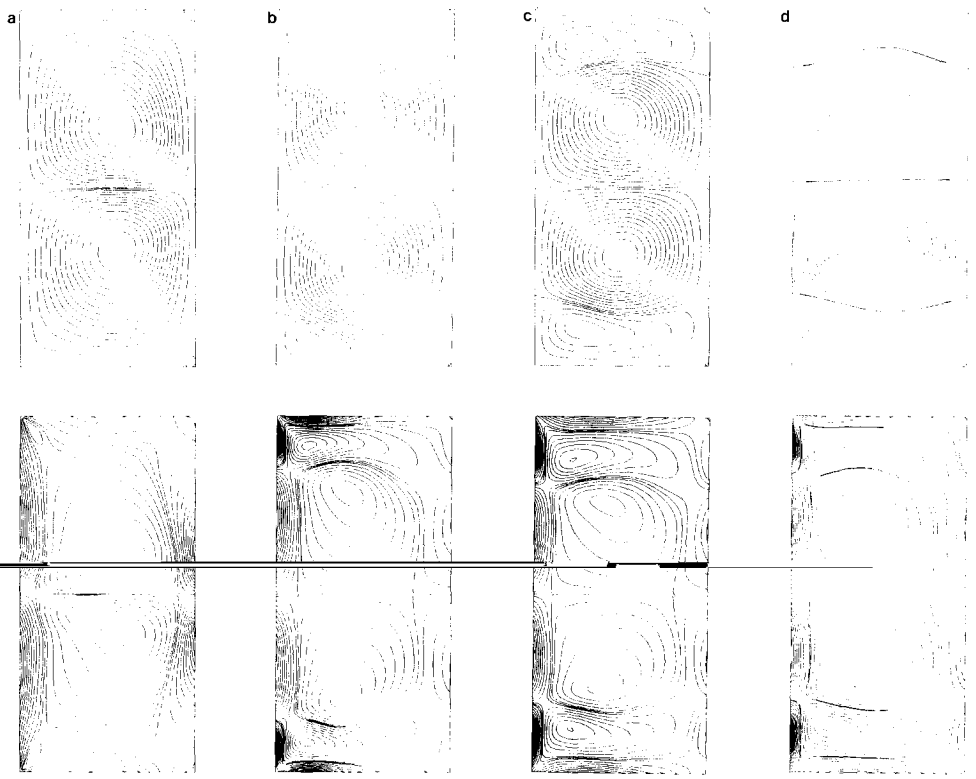

FIG. 4. Distinct finite cylinder solutions for the same physical parameters: R (Reynolds number) $= 240$, Γ (aspect ratio) $= 2$, η (radius ratio) $= 0.615$. (a)-(d) correspond to the points labelled on the schematic diagram in Fig. 2. (a) normal two-cell mode, (b), (c) anomalous two-cell modes which are symmetric in z; (d) anomalous two-cell mode which is unsymmetric in z and not stable. A fifth solution is obtained by reflection of Fig. 4d in the plane $z = \Gamma/2$ and is not shown.

Thus we have two anomalous two-cell solutions which may be stable. It is not clear which one was observed by Benjamin and Mullin [2], but we guess it was the first one, Fig. 4b, since it has smaller "hidden" vortices.

The so-called anomalous one-cell modes have already been computed by Cliffe (1983). (These consist of two unequal cells.) We obtained them independently and agree with his results.

Thus we have confirmed completely the bifurcation diagram of Fig. 2 proposed by Benjamin and Mullin for the so-called one-cell modes and the so-called anomalous two-cell modes.

Figure 5 shows an anomalous three-cell mode computed by the same procedure. A mirror image solution also exits. Figures 6a and b show two anomalous four-cell modes, computed using the symmetry in z. The first has large "hidden" vortices and the second has small ones.

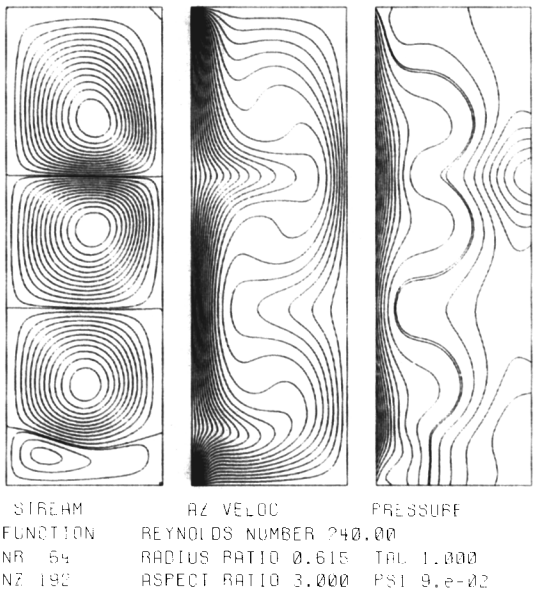

FIG. 5. Anomalous three-cell mode. The parameter values are listed on the plot. Also given is the maximum absolute value of the stream function ψ.

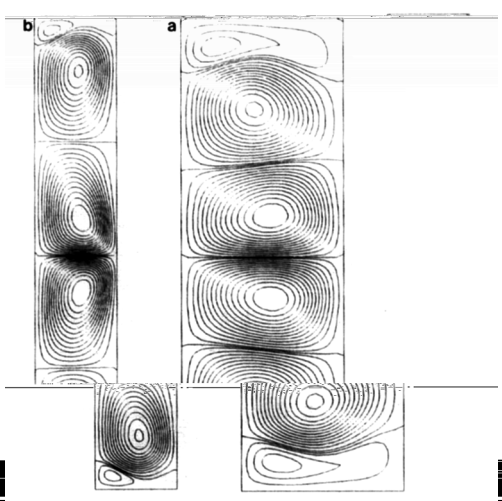

FIG. 6. Anomalous four-cell modes computed on a 25×75 grid, using symmetry. The Reynolds numbers and aspects ratios are (a) 283.92 and 2.886 and (b) 305.98 and 5.683. The extra vortices are large in the former and small in the latter.

A new phenomenon is illustrated in Fig. 7 for low aspect ratio and high Reynolds number in the anomalous two mode: the splitting of the extra vortices into two smaller vortices. We did not observe this in the other modes, but Fig. 6a points to a tendency in this direction, which might be observed at higher Reynolds numbers.

Figures 8 and 9 show anomalous five- and six-modes, respectively. Both solutions lie on their respective folds. We encountered pitchfork bifurcation points close to the folds for the anomalous four and six modes.

All these anomalous modes have extra "hidden" vortices not observed in the experiments of Benjamin and Mullin [2], but observed in the new experiments of Cliffe and Mullin [10]. These vortices become progressively smaller and weaker with increasing Reynolds number.

In Figure 10 we give a quantitative comparison of our results with the experiments of Benjamin and Mullin [2, p. 239], and with the experiments and computations of Cliffe and Mullin [10]. We note that the former authors used a Reynolds number based on inner radius, but in later papers based their Reynolds number on gap width. So all references to Reynolds number in this paper will be in terms of gap width.

Figure 10 shows six curves. The upper left solid curve is our computed locus of fold points in the aspect ratio-Reynolds number plane for the anomalous two modes. The upper middle (right) solid curve is the same, but for the anomalous three (four) modes. All calculations use radius ratio $\eta = 0.615$. The two (resp. three-, four-) modes are computed on a 33×73 (resp. 25×73, 25×73) grid. The even modes are computed on half the region using symmetry. (As mentioned above, the multigrid method was not used for these computations.) The lower left (resp. middle, right) dotted curve is the experimental two (resp. three, four) mode locus of fold points as determined by Benjamin and Mullin [2]. Our curves agree to

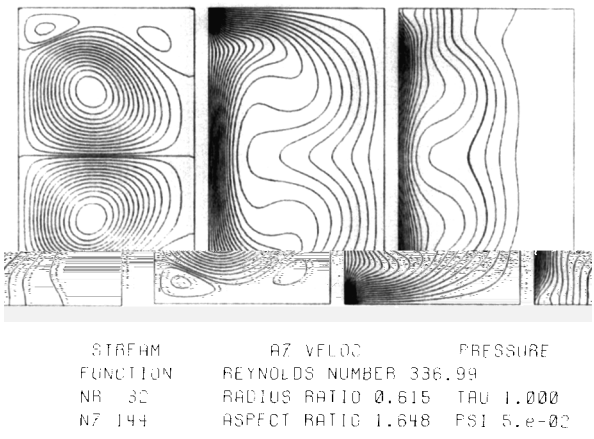

FIG. 7. Anomalous two-cell mode showing the splitting of the small vortices into two smaller vortices.

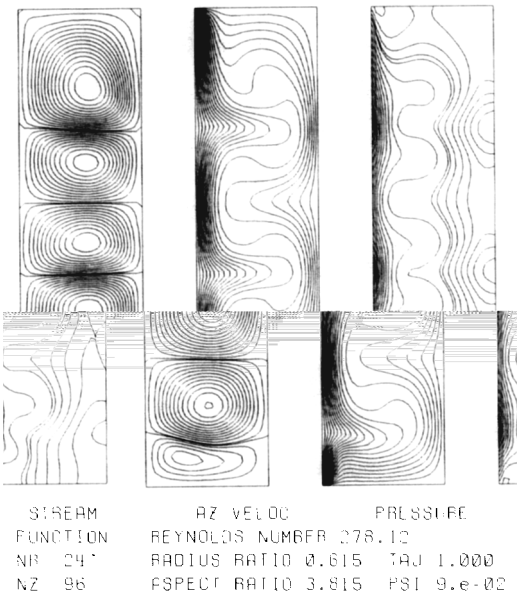

FIG. 8. Anomalous five-cell mode.

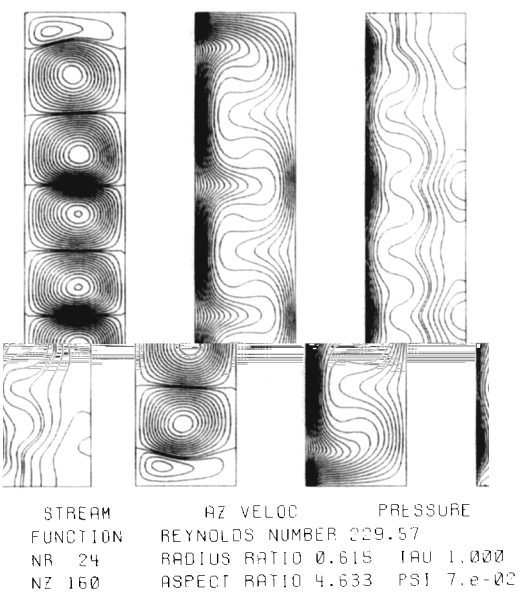

FIG. 9. Anomalous six-cell mode.

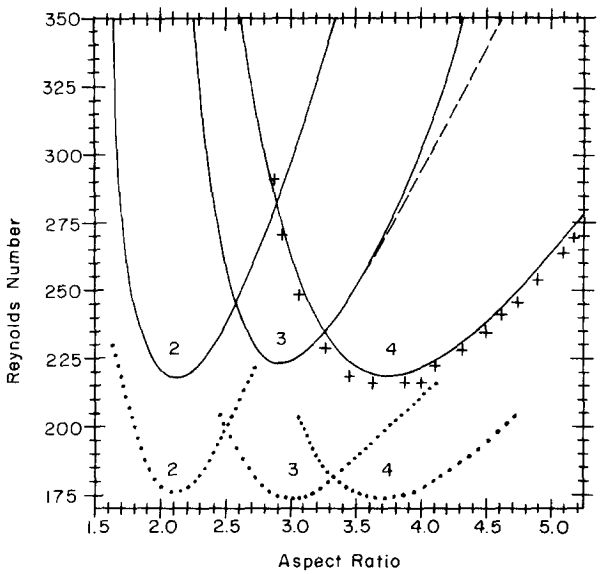

FIG. 10. Locus of limit points of anomalous two-, three-, and four-cell modes at aspect ratio $\eta = 0.615$ and comparison with experiments. The solid curves are calculated by us. To graphical accuracy they agree with the calculations of Cliffe and Mullin [10] except for the dashed portion of the three-mode curve. The dotted curves are the original (erroneous) experiments of Benjamin and Mullin [2]. The crosses are the more recent experiments of Cliffe and Mullin [10] for the anomalous four-mode at $\eta = 0.6$.

graphical accuracy with the computed folds of Cliffe and Mullin [10] except for the dashed portion of their three-mode curve. The crosses are the more recent experiments of Cliffe and Mullin for the anomalous four mode. These are not strictly comparable, since they are for aspect ratio $\eta = 0.6$ instead of 0.615 as on all the other curves.

In Figure 6 we showed two anomalous four modes. Both lie on the anomalous four fold curve, but the four-cell mode of Figure 6a (resp. 6b) lies on the left (resp. right) side of the fold. In general we find that the "hidden" vortices become smaller with increasing aspect ratio.

Qualitatively our computed curves have the same shape as those determined by the old experiments, but quantitatively there is a large discrepancy. For example, we calculated the minimum Reynolds number of our two-, three-, four-cell curve near $(\Gamma, R) = (2.12, 221), (2.92, 223), (3.75, 218)$, respectively. But from the graph in Benjamin and Mullin (1981) it appears that their minimum occurs at approximately the same aspect ratio, but at $R = 176$ (resp. 174, 172). Thus we have a disagreement of approximately 30% with the old experiments. However, we obtain very good agreement with the new experiments and the computations of Cliffe and Mullin, except for the three mode curve at large values of the aspect ratio.

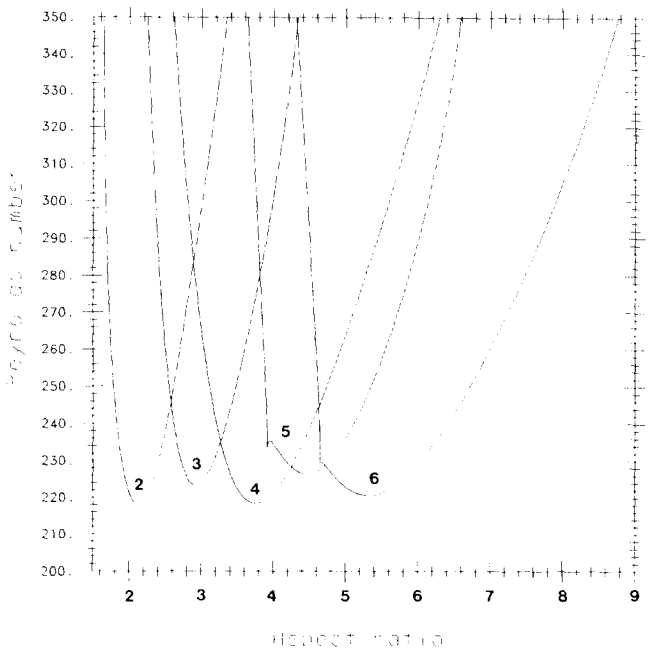

FIG. 11. Fold curves for anomalous 2, 3, 4, 5, and 6 modes. The leftmost three curves are the same as in Fig. 9. The curves for the 5 and 6 modes have a cusp at the lower left. The left side of these curves is nearly a straight line.

Figure 11 shows the computed locus of fold points in the aspect ratio-Reynolds number plane for the anomalous 2, 3, 4, 5, and 6 modes. The number of solution points used to plot these curves was 49, 82, 47, 153, and 209, respectively. The 2-, 3-, and 4-mode curves are the same as in the previous figure. The 5 and 6 modes are computed on 25×97 and 25×81 grids, respectively; the latter employing symmetry. The points of minimum Reynolds number on these curves are at $(\Gamma, R) = (4.46, 226.3)$ and $(5.31, 220.5)$, respectively. Two new geometric features arise for $n = 5$ and 6 that are not present in the other curves. The first is a cusp in the lower left part of each curve, located at (3.91, 233.5) and (4.63, 229.5), respectively. The second is the strange straight-line appearance of the left sides of the curves. In fact, they are almost straight lines. We have checked them by computing the 5 mode curve on a different grid. As a further test we continued off the fold, holding one parameter fixed, then continued in the other parameter until a limit point was detected. We verified that the previously computed fold went through this limit point. For example, we started at fold point $R = 402.51$, $\Gamma = 3.720$ and continued in increasing aspect ratio until $\Gamma = 3.857$. Then we fixed Γ and continued in decreasing Reynolds number until we detected the limit point at $R = 261.9$. During fold-following, we had obtained the nearby fold points $(\Gamma, R) = (3.849, 265.1)$ and $(3.863, 259.6)$. Interpolating linearly at $\Gamma = 3.857$ we obtained $R = 261.9$, in

TABLE I

Location of Minimum Reynolds Number of Fold for Anomalous Two-Modes by Repeated Richardson Extrapolation.

N_r	N_z	Computed Reynolds number	Extrapolated Reynolds number (order) 4	6	8
16	36	210.204			
20	45	213.264	218.704		
24	54	215.261	219.800	220.676	
28	63	216.588	220.265	220.750	220.786
32	72	217.501	220.480	220.757	220.762

agreement with the limit point just found. This procedure was repeated three times on different parts of the "straight line" portion of the curve with the same result.

Our step control mechanism [5] enables us to continue through the cusps without human intervention in the program. We monitor the angle between successive tangent vectors as well, which provides additional evidence of the cusps.

To gauge the accuracy of our computed folds, we locate the minimum Reynolds number of the fold of the anomalous two-mode (the upper left curve in Fig. 10) on a sequence of grids, and perform repeated Richardson extrapolation. Brent's [8] derivative-free one-dimensional minimizer Localmin is used here. The results are shown in Table I. The first two columns show the number of intervals in the r and z directions. (Symmetry is used here.) The third column gives the computed Reynolds number of the minimum point of the fold. Column 4, 5, and 6 give the results of Richardson extrapolation to orders 4, 6, and 8, respectively. Our basic calculation appears to be *globally* second order accurate, as we have assumed. Furthermore, the location of the minimum appears to be at $R = 220.8$ with an error of at most one unit in the last place. A similar Richardson procedure on the aspect ratio yields an extrapolated value $\Gamma = 2.12$. We also extrapolated a different set of grids with the same results. (We did not use Richardson extrapolation to determine the minimum Reynolds number of the other folds.)

The reason for our disagreement with Cliffe and Mullin for large aspect ratios in the anomalous 3 fold may be related to the discontinuities in the stream function at the top and bottom of the inner cylinder. Cliffe and Mullin used refined finite elements at these locations. Although we believe both our calculations are second order accurate, we require more grid points than they do to obtain the same results. The large aspect ratios are the ones which require the most grid points, and this is where we disagree. The odd modes are the ones where the disagreement appears because the symmetry in the even modes effectively yields a doubling of the number of grid points in the z direction.

6. Conclusions and Extensions

From this work we draw four conclusions. First, our computations suggest phenomena (extra vortices) that may have been overlooked in experiments. Second, we have numerically confirmed Schaeffer's use of homotopy, and Benjamin and Mullin's adoption of this method to obtain the structure of the bifurcation diagram for the anomalous two-modes. Third, our computations are in qualitative agreement with the experiments of Benjamin and Mullin for the fold of anomalous two-, three-, and four-modes, and in quantitative agreement with the more recent experiments of Cliffe and Mullin. Finally, we have shown that the multigrid method can be used with the pseudo-arc-length continuation procedure to yield a powerful technique for solving bifurcation problems in fluid dynamics. Indeed, the multigrid method can be considered as continuation in the grid size.

Some extensions of the current work are immediately suggested. Near the top and bottom of the inner cylinder uniform, nested (multilevel) refinements should be used [7]. The fold-following algorithm of Section 3 should be extended to use multigrid. We can also increase the order of accuracy from second to fourth order using tau extrapolation (deferred correction) [6], at least for periodic flows. Work is in progress in these areas.

Acknowledgments

We are grateful to the IBM Corporation for support of the Applied Math-IBM 4341 at Caltech. We thank Geza Schrauf for many technical discussions, and Nathan Dinar and the referees for carefully reading the manuscript.

References

1. T. B. Benjamin, *Proc. Roy. London Ser. A* **359** (1978), 1.
2. T. B. Benjamin and T. Mullin, *Proc. Roy. London Ser. A* **377** (1981), 221.
3. T. B. Benjamin and T. Mullin, *J. Fluid Mech.* **121** (1982), 219.
4. J. H. Bolstad and H. B. Keller, "Taylor Vortex Flows by Multigrid Methods," SIAM National meeting, Seattle, Washington, July 16–20, 1984.
5. J. H. Bolstad and H. B. Keller, *SIAM J. Sci. Stat. Comput.* **7** (1986), 1081.
6. A. Brandt, "Guide to Multigrid Development," in *Multigrid Methods*, edited by W. Hackbusch and U. Trottenberg, Lecture Notes in Mathematics, No. 960, (Springer–Verlag, New York, 1982), p. 220.
7. A. Brandt, "Multilevel Adaptive Techniques (*MLAT*) for Partial Differential Equations: Ideas and Software," in "*Mathematical Software III*," edited by J. Rice (Academic Press, New York, 1977), p. 277.
8. R. Brent, *Algorithms for Minimization without Derivatives* (Prentice–Hall, Englewood Cliffs, N. J., 1973), p. 182.
9. K. A. Cliffe, *J. Fluid Mech.* **135** (1983), 219.
10. K. A. Cliffe and T. Mullin, *J. Fluid Mech.* **153** (1985), 243.
11. K. A. Cliffe and A. Spence, "The Calculation of High Order Singularities in the Finite Taylor Problem," in *Numerical Methods for Bifurcation Problems*, edited by T. Küpper, H. D. Mittlemann, and H. Weber (Birkhäuser, Boston, 1984), p. 129.

12. J. J. DONGARRA, J. R. BUNCH, C. B. MOLER, AND G. W. STEWART, LINPACK *Users' Guide* (Society for Industrial and Applied Mathematics, Philadelphia, 1979), p. 2.1.
13. H. FASEL AND O. BOOZ, *J. Fluid Mech.* **138** (1984), 21.
14. J. FIER AND H. B. KELLER, "Follow the Folds: the Flow Between Rotating Disks," in preparation.
15. J. FIER, "Fold Continuation and the Flow Between Rotating, Coaxial Disks," Ph. D. thesis, California Institute of Technology, Passadena, 1985. (unpublished).
16. S. GOLDSTEIN, *Modern Developments in Fluid Dynamics* (Dover, New York, 1938), p. 115.
17. I. P. JONES AND K. A. CLIFFE, "Numerical Solutions for the Flow due to Rotating Cylinders and Disks," Fifth Workshop on Gases under Strong Rotation, University of Virginia, Charlottesville, Va., June 1983.
18. H. B. KELLER, "Numerical Solution of Bifurcation and Nonlinear Eigenvalue Problems," in *Applications of Bifurcation Theory*, edited by P. Rabinowitz (Academic Press, New York, 1977), p. 359.
19. P. S. MARCUS, *J. Fluid Mech.* **146** (1984), 45.
20. R. MEYER-SPASCHE AND H. B. KELLER, *J. Comput. Phys.* **35** (1980), 100.
21. R. MEYER-SPASCHE AND H. B. KELLER, "Numerical Study of Taylor-Vortex Flows Between Rotating Cylinders II," Caltech Report, 1982 (unpublished).
22. G. MOORE AND A. SPENCE, *SIAM J. Numer. Anal.* **17** (1980), 567.
23. G. P. NEITZEL, *J. Fluid Mech.* **141** (1984), 51.
24. D. SCHAEFFER, *Math. Proc. Cambridge Phitos. Soc.* **87** (1980), 307.
25. J. C. STRIKWERDA, "A Numerical Study of Taylor-Vortex Flow," Mathematics Research Center, University of Wisconin, Technical Report No. 2808, April 1985.
26. K. STUEBEN AND U. TROTTENBERG, "Multigrid Methods: Fundamental Algorithms, Model Problem Analysis and Applications," in *Multigrid Methods*, edited by W. Hackbusch and U. Trottenberg, Lecture Notes in Mathematics, No. 960. (Springer-Verlag, New York, 1982), p. 1.
27. G. I. TAYLOR, *Philos. Trans. Roy. Soc. London Ser. A* **223** (1923), 289.